

Final results on neutrino oscillation parameters from the OPERA experiment in the CNGS beam

N. Agafonova,¹ A. Alexandrov,² A. Anokhina,³ S. Aoki,⁴ A. Ariga,⁵ T. Ariga,^{5,6} A. Bertolin,⁷ C. Bozza,⁸ R. Brugnera,^{7,9} S. Buontempo,² M. Chernyavskiy,¹⁰ A. Chukanov,¹¹ L. Consiglio,² N. D'Ambrosio,¹² G. De Lellis,^{2,13,14} M. De Serio,^{15,16} P. del Amo Sanchez,¹⁷ A. Di Crescenzo,^{2,13} D. Di Ferdinando,¹⁸ N. Di Marco,¹² S. Dmitrievsky,¹¹ M. Dracos,¹⁹ D. Duchesneau,¹⁷ S. Dusini,⁷ T. Dzhatdoev,³ J. Ebert,²⁰ A. Ereditato,⁵ R. A. Fini,¹⁶ T. Fukuda,²¹ G. Galati,^{2,13} A. Garfagnini,^{7,9} V. Gentile,²² J. Goldberg,²³ S. Gorbunov,¹⁰ Y. Gornushkin,¹¹ G. Grella,⁸ A. M. Guler,²⁴ C. Gustavino,²⁵ C. Hagner,²⁰ T. Hara,⁴ T. Hayakawa,²¹ A. Hollnagel,²⁰ K. Ishiguro,²¹ A. Iuliano,^{2,13} K. Jakovčić,²⁶ C. Jollet,¹⁹ C. Kamiscioglu,^{24,27} M. Kamiscioglu,²⁴ S. H. Kim,²⁸ N. Kitagawa,²¹ B. Kliček,^{29,*} K. Kodama,³⁰ M. Komatsu,²¹ U. Kose,^{7,†} I. Kreslo,⁵ F. Laudisio,^{7,9} A. Lauria,^{2,13} A. Longhin,^{7,9} P. Loverre,²⁵ A. Malgin,¹ G. Mandrioli,¹⁸ T. Matsuo,³¹ V. Matveev,¹ N. Mauri,^{18,32} E. Medinaceli,^{7,9,‡} A. Mereaglia,¹⁹ S. Mikado,³³ M. Miyanishi,²¹ F. Mizutani,⁴ P. Monacelli,²⁵ M. C. Montesi,^{2,13} K. Morishima,²¹ M. T. Muciaccia,^{15,16} N. Naganawa,²¹ T. Naka,³¹ M. Nakamura,²¹ T. Nakano,²¹ K. Niwa,²¹ S. Ogawa,³¹ N. Okateva,¹⁰ K. Ozaki,⁴ A. Paoloni,³⁴ L. Paparella,^{15,16} B. D. Park,^{28,§} L. Pasqualini,^{18,32} A. Pastore,¹⁶ L. Patrizii,¹⁸ H. Pessard,¹⁷ D. Podgrudkov,³ N. Polukhina,^{10,35} M. Pozzato,¹⁸ F. Pupilli,⁷ M. Roda,^{7,9,||} T. Roganova,³ H. Rokujo,²¹ G. Rosa,²⁵ O. Ryazhskaya,¹ O. Sato,²¹ A. Schembri,¹² I. Shakiryanova,¹ T. Shchedrina,¹⁰ E. Shibayama,⁴ H. Shibuya,³¹ T. Shiraiishi,²¹ S. Simone,^{15,16} C. Sirignano,^{7,9} G. Sirri,¹⁸ A. Sotnikov,¹¹ M. Spinetti,³⁴ L. Stanco,⁷ N. Starkov,¹⁰ S. M. Stellacci,⁸ M. Stipčević,²⁹ P. Strolin,^{2,13} S. Takahashi,⁴ M. Tenti,^{18,*} F. Terranova,³⁶ V. Tioukov,² S. Tufanli,^{5,¶} S. Vasina,¹¹ P. Vilain,³⁷ E. Voevodina,² L. Votano,³⁴ J. L. Vuilleumier,⁵ G. Wilquet,³⁷ and C. S. Yoon²⁸

(OPERA Collaboration)

¹INR—Institute for Nuclear Research of the Russian Academy of Sciences, RUS-117312 Moscow, Russia

²INFN Sezione di Napoli, I-80126 Napoli, Italy

³SINP MSU—Skobeltsyn Institute of Nuclear Physics, Lomonosov Moscow State University, RUS-119991 Moscow, Russia

⁴Kobe University, J-657-8501 Kobe, Japan

⁵Albert Einstein Center for Fundamental Physics, Laboratory for High Energy Physics (LHEP), University of Bern, CH-3012 Bern, Switzerland

⁶Faculty of Arts and Science, Kyushu University, J-819-0395 Fukuoka, Japan

⁷INFN Sezione di Padova, I-35131 Padova, Italy

⁸Dipartimento di Fisica dell'Università di Salerno and “Gruppo Collegato” INFN, I-84084 Fisciano (Salerno), Italy

⁹Dipartimento di Fisica e Astronomia dell'Università di Padova, I-35131 Padova, Italy

¹⁰LPI—Lebedev Physical Institute of the Russian Academy of Sciences, RUS-119991 Moscow, Russia

¹¹JINR—Joint Institute for Nuclear Research, RUS-141980 Dubna, Russia

¹²INFN—Laboratori Nazionali del Gran Sasso, I-67010 Assergi (L'Aquila), Italy

¹³Dipartimento di Fisica dell'Università Federico II di Napoli, I-80126 Napoli, Italy

¹⁴CERN, European Organization for Nuclear Research, Geneva, Switzerland

¹⁵Dipartimento di Fisica dell'Università di Bari, I-70126 Bari, Italy

¹⁶INFN Sezione di Bari, I-70126 Bari, Italy

¹⁷LAPP, Université Savoie Mont Blanc, CNRS/IN2P3, F-74941 Annecy-le-Vieux, France

¹⁸INFN Sezione di Bologna, I-40127 Bologna, Italy

¹⁹IPHC, Université de Strasbourg, CNRS/IN2P3, F-67037 Strasbourg, France

²⁰Hamburg University, D-22761 Hamburg, Germany

²¹Nagoya University, J-464-8602 Nagoya, Japan

²²GSSI—Gran Sasso Science Institute, I-40127 L'Aquila, Italy

²³Department of Physics, Technion, IL-32000 Haifa, Israel

²⁴METU—Middle East Technical University, TR-06800 Ankara, Turkey

²⁵INFN Sezione di Roma, I-00185 Roma, Italy

²⁶Ruđer Bošković Institute, HR-10000 Zagreb, Croatia

²⁷Ankara University, TR-06560 Ankara, Turkey

²⁸Gyeongsang National University, 900 Gazwa-dong, Jinju 660-701, Korea

²⁹Center of Excellence for Advanced Materials and Sensing Devices, Ruđer Bošković Institute, HR-10000 Zagreb, Croatia

³⁰*Aichi University of Education, J-448-8542 Kariya (Aichi-Ken), Japan*³¹*Toho University, J-274-8510 Funabashi, Japan*³²*Dipartimento di Fisica e Astronomia dell'Università di Bologna, I-40127 Bologna, Italy*³³*Nihon University, J-275-8576 Narashino, Chiba, Japan*³⁴*INFN—Laboratori Nazionali di Frascati dell'INFN, I-00044 Frascati (Roma), Italy*³⁵*MEPhI—Moscow Engineering Physics Institute, RUS-115409 Moscow, Russia*³⁶*Dipartimento di Fisica dell'Università di Milano-Bicocca, I-20126 Milano, Italy*³⁷*IHE, Université Libre de Bruxelles, B-1050 Brussels, Belgium*

(Received 12 April 2019; published 6 September 2019)

The OPERA experiment has conclusively observed the appearance of tau neutrinos in the muon neutrino CNGS beam. Exploiting the OPERA detector capabilities, it was possible to isolate high purity samples of ν_e , ν_μ and ν_τ charged current weak neutrino interactions, as well as neutral current weak interactions. In this paper, the full dataset is used for the first time to test the three-flavor neutrino oscillation model and to derive constraints on the existence of a light sterile neutrino within the framework of the $3 + 1$ neutrino model. For the first time, tau and electron neutrino appearance channels are jointly used to test the sterile neutrino hypothesis. A significant fraction of the sterile neutrino parameter space allowed by LSND and MiniBooNE experiments is excluded at 90% C.L. In particular, the best-fit values obtained by MiniBooNE combining neutrino and antineutrino data are excluded at 3.3σ significance.

DOI: [10.1103/PhysRevD.100.051301](https://doi.org/10.1103/PhysRevD.100.051301)

I. INTRODUCTION

The OPERA experiment [1] was designed to conclusively observe the appearance of tau neutrino in the high purity muon neutrino CNGS beam [2,3], in the parameter region indicated by Super-Kamiokande [4] and MACRO [5] to explain the zenith dependence of the atmospheric neutrino deficit. The average neutrino energy in the CNGS beam was designed to be about 17 GeV, the $\bar{\nu}_\mu$ fraction was 2.1% in terms of expected charged current (CC) interactions, the sum of the ν_e and $\bar{\nu}_e$ fractions was below 1%, while the prompt ν_τ component was negligible.

The OPERA detector [1] was located in the underground Gran Sasso Laboratory (LNGS), about 730 km away from the neutrino source at CERN. The detector was a hybrid apparatus made of a nuclear emulsion/lead target complemented by electronic detectors (ED) [6]. The target had a total mass of about 1.25 kt and was composed of two identical sections. Each section consisted of 31 walls of emulsion cloud chamber (ECC) bricks, interleaved by

planes of horizontal and vertical scintillator strips (target tracker) used to select [7] ECC bricks in which a neutrino interaction had occurred. Each ECC brick consisted of 57 emulsion films interleaved with 1 mm thick lead plates, with a (12.7×10.2) cm² cross section and a total thickness corresponding to about ten radiation lengths. A magnetic muon spectrometer [1,8] was positioned downstream of each target section, and was instrumented by resistive plate chambers and high-resolution drift tubes.

The experiment collected data from the CNGS beam from 2008 to 2012, with an integrated exposure of 17.97×10^{19} protons on target. A total of 19505 neutrino interaction events in the target were recorded by the electronic detectors, of which 5603 were fully reconstructed in the OPERA emulsion films.

In 2015, the OPERA Collaboration reported the discovery of tau neutrino appearance [9]. Five ν_τ candidate events [9–13] were observed, with an expected signal-to-background ratio of ~ 10 . The analysis of these data lead to the exclusion of the background-only hypothesis with a significance of 5.1σ .

The final result on ν_τ appearance was published in 2018 [14], using an analysis based on a multivariate approach and a looser selection with respect to [9], applied to the complete data set. The achieved significance for tau appearance was 6.1σ . Additionally, the atmospheric neutrino mass splitting was measured to be $|\Delta m_{32}^2| = 2.7_{-0.6}^{+0.7} \times 10^{-3}$ eV², assuming maximal two-flavor mixing.

A search for electron neutrino CC interactions was performed [15,16]. Unlike ν_τ appearance, the sensitivity to the $\nu_\mu \rightarrow \nu_e$ oscillation channel is limited mainly by the ν_e beam contamination and the systematic uncertainty in the neutrino flux. The collected sample of electron

*Corresponding authors: budimir.klicek@irb.hr, matteo.tenti@bo.infn.it

†Now at CERN.

‡Now at INAF—Osservatorio Astronomico di Padova, Padova, Italy.

§Now at Samsung Changwon Hospital, SKKU, Changwon, Korea.

||Now at University of Liverpool, Liverpool, United Kingdom.

¶Now at Yale University New Haven, CT 06520, USA

Published by the American Physical Society under the terms of the [Creative Commons Attribution 4.0 International license](https://creativecommons.org/licenses/by/4.0/). Further distribution of this work must maintain attribution to the author(s) and the published article's title, journal citation, and DOI. Funded by SCOAP³.

neutrino candidates was in agreement with the expectation from the three-flavor neutrino mixing model and was exploited to obtain a 90% C.L. upper limit on the parameter $\sin^2 2\theta_{13} < 0.43$ [16].

The data were also used to test the hypothesis of one additional light sterile neutrino state, in the $3 + 1$ neutrino mixing model [15–17]. OPERA is sensitive to a significant part of the allowed region of the sterile neutrino parameters defined by the LSND [18] and MiniBooNE [19] experiments, and to a large part of the yet unexplored neutrino parameter space related to ν_τ - ν_s mixing.

In this paper, the final samples of tau and electron neutrino CC interactions are used for the first time in a combined analysis to constrain standard oscillation parameters θ_{13} , θ_{23} , as well as the $3 + 1$ mixing model ones. In addition, a search for the ν_μ disappearance signal was performed using only electronic detector data, assuming three-flavor neutrino mixing.

II. DATA SELECTION

A. Selection of ν_τ and ν_e CC candidate events using emulsion detector data

The emulsion detector data set consists of events in which the neutrino interaction vertex is fully reconstructed in the emulsion films. Tracking capabilities of the OPERA emulsion technique allow isolating samples of tau and electron neutrino CC interactions with a very high signal-to-background ratio [11,20]. In the final analysis, ten tau neutrino candidates have been identified [14], while the expected background amounts to 2.0 ± 0.4 events. The sources of background are: (i) the decay of charmed particles produced in ν_μ CC interactions, (ii) the reinteraction of hadrons from ν_μ events in lead, and (iii) the large-angle scattering (LAS) of muons produced in ν_μ CC interactions. Processes (i) and ν_μ CC in (ii) represent a background source when the μ^- at the primary vertex is not identified.

The search for electron neutrino appearance led to the selection of 35 ν_e candidates in the full dataset resulting from a dedicated analysis [16]. The two main sources of background are (i) ν_τ CC interactions followed by a $\tau \rightarrow e$ decay and (ii) muonless events with a $\pi^0 \rightarrow \gamma\gamma$ decay and an e^+e^- pair from prompt γ conversion misidentified as an electron. The total expected background amounts to 1.2 ± 0.5 events. Given the prompt ν_e and $\bar{\nu}_e$ beam components, the number of observed ν_e events is consistent both with no-oscillation (31.9 ± 3.3) and standard oscillation (34.3 ± 3.5) hypotheses with normal neutrino mass hierarchy (NH) [16].

B. Selection of ν_μ CC and ν NC candidate events using only electronic detector data

Only electronic detector data were used in a search for ν_μ disappearance, since events without a decay topology (most

of ν_μ CC interactions and ν NC interactions) are not fully reconstructed in the emulsion target [20]. This analysis is complementary to the appearance study, as this dedicated selection of ED data differs from the one used to locate ECC bricks in which ν interactions occurred.

The compositions of CC-like and NC-like samples described below were estimated using standard Monte Carlo simulation validated on data [6], with GENIE v2.8.6 [21,22] as a neutrino interaction generator.

A global selection was applied to ED data: (i) the interaction vertex must be reconstructed inside the active volume defined in [23], (ii) a fiducial volume cut rejecting events in which neutrinos most probably interacted in the 10 brick walls immediately downstream of a spectrometer, and (iii) a cut on the total signal recorded by electronic detectors in order to reject soft nonbeam events.

The ν_μ CC interaction candidates (CC-like sample) are selected by requiring a muon track with negative charge reconstructed in at least two arms of a single magnetic spectrometer. According to the Monte Carlo simulation, the expected purity of the ν_μ CC-like event sample is 99.5%, and it contains 46% of expected ν_μ CC interactions in the target.

The neutrino NC interaction candidates (NC-like sample) are selected by requiring no track identified as a muon. Assuming global best-fit values of the standard oscillation parameters for NH (Table 14.1 in [24]), the MC expectation is that 75.3% of events are ν and $\bar{\nu}$ NC interactions, 20.2% are ν_μ and $\bar{\nu}_\mu$ CC interactions in which no muon was identified, and 4.5% are CC interactions of other neutrino flavors. The latter are expected to be (i) prompt ν_e and $\bar{\nu}_e$ beam components, and (ii) flavors appearing through neutrino oscillations, most significantly in channels $\nu_\mu \rightarrow \nu_\tau$ and $\nu_\mu \rightarrow \nu_e$. This sample contains 34% of expected NC interactions in the target.

NC-like and CC-like data samples consist of 1724 and 5782 events, respectively.

It should be noted that the estimated composition of NC-like and CC-like samples quoted above do not explicitly enter the analysis, as the appropriate oscillation probability is applied to all MC events as described in the next section.

III. ANALYSIS

A. Appearance analyses

Visible neutrino energy as defined in [14] and reconstructed neutrino energy as defined in [16] are used as observables for tau and electron neutrino samples, respectively. Their distributions are jointly exploited to test neutrino oscillation phenomena both in standard three-flavor and $3 + 1$ mixing models.

The expected distributions are evaluated using GLOBES [25,26]. The smearing matrices, incorporating the detection and selection efficiencies, are calculated by means of MC simulation of the full analysis chain. The simulated CNGS

flux [27], default neutrino interaction cross sections evaluated by GENIE v2.8.6 [21,22], and the smearing matrices are used as input. It is worth noting that the oscillations of all CNGS beam components (ν_μ , $\bar{\nu}_\mu$, ν_e and $\bar{\nu}_e$) are taken into account.

The systematic uncertainty on the expected number of tau neutrino candidates is largely dominated by the limited knowledge of the ν_τ CC interaction cross section and detection efficiency, overall estimated to be 20% [14].

The expected number of electron neutrino candidates is affected by systematic uncertainties on: (i) the prompt flavor beam components, (ii) the ν_e and $\bar{\nu}_e$ CC interaction cross sections, and (iii) the neutrino detection efficiency. The systematic error on the expected number of electron neutrino candidates is estimated to be 20% for reconstructed energies below 10 GeV and 10% otherwise [16].

The statistical analysis of the data is based on a maximum-likelihood joint fit across the two samples. The data are binned and the overall likelihood (\mathcal{L}) is constructed as the product of the contribution for each data sample (\mathcal{L}_τ , \mathcal{L}_e) and a Gaussian constraint \mathcal{G} on Δm_{31}^2 as:

$$\mathcal{L} = \mathcal{L}_e \times \mathcal{L}_\tau \times \mathcal{G}(\overline{\Delta m_{31}^2} | \mu_{31}, \overline{\sigma_{31}}), \quad (1)$$

where $\overline{\Delta m_{31}^2}$ and $\overline{\sigma_{31}}$ are the best fit value and the 1σ uncertainty from a global fit of the current neutrino oscillation data (Table 14.1 in [24]). The used values for $\overline{\Delta m_{31}^2} \pm \overline{\sigma_{31}}$ are $(2.56 \pm 0.05) \times 10^{-3} \text{ eV}^2$ and $(-2.49 \pm 0.05) \times 10^{-3} \text{ eV}^2$ for NH and inverted hierarchy (IH), respectively. The floating parameter μ_{31} represents the true value of the squared mass difference.

The negative log-likelihood functions $-\ln \mathcal{L}_x$ are defined as:

$$-\ln \mathcal{L}_x = \sum_{i=1}^{N^{(x)}} \left(\mu_i^{(x)} - n_i^{(x)} \ln \mu_i^{(x)} \right) + \frac{1}{2} \sum_{j=1}^{n_{\text{sys}}^{(x)}} \left(\frac{\phi_j^{(x)} - \hat{\phi}_j^{(x)}}{\sigma_{\phi_j}^{(x)}} \right)^2, \quad (2)$$

with $x = \tau$ or e , $N^{(x)}$ is the number of bins, n_i is the number of events in the i th bin of the data histogram, and $\mu_i = \mu_i(\bar{\theta}, \bar{\phi})$ is the expected number of events in the i th bin from the set of oscillations parameters $\bar{\theta}$, namely the mixing matrix elements $U_{\alpha\beta}$ and the squared mass splittings Δm_{ij}^2 , and the set of parameters $\bar{\phi}$ which account for systematic uncertainties. The second term of Eq. (2) accounts for the *a priori* knowledge of the systematic uncertainties, where $\hat{\phi}_j$ and σ_{ϕ_j} are respectively the estimated value and the uncertainty on parameter ϕ_j . The nonzero value of Δm_{21}^2 is taken into account as well as matter effects assuming a constant Earth crust density estimated with

the PREM [28,29] onion shell model, even though they were checked to be negligible for $\Delta m_{41}^2 > 1 \text{ eV}^2$.

B. Disappearance analysis

A search for the ν_μ disappearance signal is performed in the dedicated ED data sample. Since the experiment was not equipped with a near detector, the uncertainty on the ν_μ flux is estimated to be 15%. On the other hand, the detector was located far from the first oscillation maximum, so that the ν_μ CC rate reduction at the detector due to oscillation does not exceed 2% in the standard 3-flavor model. To overcome these difficulties, a NC-like/CC-like event rate ratio is used as an estimator of the disappearance oscillation probability that is independent from the overall flux normalization uncertainty.

Since it is experimentally unfeasible to reconstruct the energy of an incoming neutrino in NC events, NC-like/CC-like event rate is evaluated as a function of a measurement of the energy deposited in the target, denoted by E_T .

In order to constrain the value of the atmospheric mass splitting Δm_{32}^2 , three histograms with identical binning in E_T are constructed: (i) the predicted NC-like/CC-like ratio evaluated using MC simulation as a function of Δm_{32}^2 , (ii) the observed number of CC-like events, (iii) the observed number of NC-like events.

While constructing histogram (i), global best-fit values (Table 14.1 in [24]) for all oscillation parameters except the parameter of interest Δm_{32}^2 are used, separately for NH and IH. For each value of Δm_{32}^2 , a proper oscillation probability is calculated for each simulated event in both NC-like and CC-like samples, including disappearance of ν_μ , $\bar{\nu}_\mu$, ν_e and $\bar{\nu}_e$ CC interactions and $\nu_\mu \rightarrow \nu_\tau$ and $\nu_\mu \rightarrow \nu_e$ appearance.

A dedicated statistical model is built to properly construct confidence intervals based on a ratio of two Poisson random variables. Given two outcomes l and k of two Poisson distributions with mean values λ_l and λ_k , respectively, the Bayesian probability of ratio $x \equiv \lambda_l/\lambda_k$, assuming a flat prior on x , is provided by the formula

$$P_{l/k}(x) = \frac{(k+l+1)!}{k!l!} \frac{x^l}{(1+x)^{k+l+2}}. \quad (3)$$

The likelihood function is constructed as

$$L(\Delta m_{32}^2) = \prod_{j=1}^N P_{\text{NC}_j/\text{CC}_j}(R_j(\Delta m_{32}^2)), \quad (4)$$

where j is a bin label running on all three histograms; NC_j and CC_j are the j th bin content of the NC-like (ii) and CC-like (iii) histograms, respectively; $R_j(\Delta m_{32}^2)$ is the NC-like/CC-like ratio obtained from histogram (i) as a function of

oscillation parameters; $P_{\text{NC}_j/\text{CC}_j}(x)$ is a probability distribution defined in Eq. (3).

In order to extract the confidence interval, the upper limit test statistic [30] is used, defined by equation

$$q_{\Delta m_{32}^2} = \begin{cases} -2 \ln \frac{L(\widehat{\Delta m_{32}^2})}{L(\Delta m_{32}^2)} & \widehat{\Delta m_{32}^2} \leq \Delta m_{32}^2 \\ 0 & \widehat{\Delta m_{32}^2} > \Delta m_{32}^2 \end{cases}, \quad (5)$$

where $\widehat{\Delta m_{32}^2}$ is the value of Δm_{32}^2 which maximizes the likelihood function $L(\Delta m_{32}^2)$. A complete treatment of the statistical model can be found in [31].

The effect of uncorrelated uncertainties in the knowledge of the CNGS flux is estimated by dividing the simulated neutrino events into subsets (bins) according to true neutrino energy. The bins are 10 GeV wide, and the weight of every event in a single bin is multiplied by the same Gaussian random number with mean value of 1 and standard deviation of 0.15, corresponding to the uncertainty on the total neutrino flux. Event weights in different bins are multiplied by different random numbers from the same Gaussian distribution. A set of 1000 different smeared fluxes is generated in this way for each value of Δm_{32}^2 .

The likelihood function is modified to take into account these multiple smeared fluxes as follows:

$$L(\Delta m_{32}^2) = \prod_{i=1}^N \left(\frac{1}{M} \sum_{j=1}^M P_{\text{NC}_i/\text{CC}_i}(R_i^{(j)}(\Delta m_{32}^2)) \right), \quad (6)$$

where M is the number of smeared fluxes, and $R_i^{(j)}(\Delta m_{32}^2)$ is a MC predicted NC-like over CC-like event ratio in the i th E_T bin obtained using j th smeared input flux.

IV. RESULTS

A. Standard three-flavor model

Appearance channels are jointly used to obtain constraints on three-flavor model parameters θ_{23} and θ_{13} . All other parameters are treated as nuisance and the profile likelihood ratio is used to remove the dependence of the likelihood [Eq. (1)] on them. The 68% C.L. allowed region for NH, obtained using Wilks' theorem, is reported in Fig. 1. Resulting best fit value and 1σ confidence interval for θ_{23} parameter are $\theta_{23} = 0.78_{-0.31}^{+0.32}$ rad; the 1σ confidence interval for θ_{13} is $[0, 0.20]$ rad. The best fit value of the constrained parameter Δm_{31}^2 is 2.56×10^{-2} eV².

The $\nu_\mu \rightarrow \nu_\mu$ disappearance channel was explored using the test statistic [Eq. (5)] based on the likelihood [Eq. (4)] to obtain an upper limit on Δm_{32}^2 . The values of Δm_{32}^2 are sampled on a grid in the interval $[0.0, 6.0] \times 10^{-3}$ eV² for NH, and $[-6.0, 0.0] \times 10^{-3}$ eV² for IH. In both cases, the grid spacing is 6.0×10^{-5} eV². The distribution of $q_{\Delta m_{32}^2}$

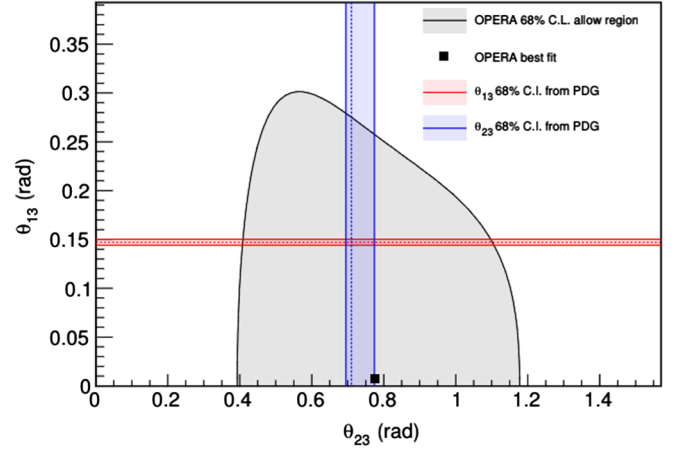


FIG. 1. OPERA 68% C.L. allowed region in the θ_{13} and θ_{23} parameter space for the normal hierarchy of the three standard neutrino masses. Red and blue dashed lines (areas) represent 1σ confidence interval obtained from the global best fit values (Table 14.1 in [24], 3σ allowed ranges) for θ_{13} and θ_{23} respectively.

[Eq. (5)] is calculated for each of these grid points using 10 000 pseudoexperiments. This is then used to calculate a p -value for each point for both NH and IH cases, shown in Fig. 2 as “no smearing” curves. For both NH and IH assumptions, the 90% confidence interval is given as $|\Delta m_{32}^2| < 4.1 \times 10^{-3}$ eV².

The p -values obtained using smeared neutrino fluxes by using likelihood [Eq. (6)] are shown in Fig. 2 as “with smearing” curves. There is no significant difference with respect to p -values obtained without smearing.

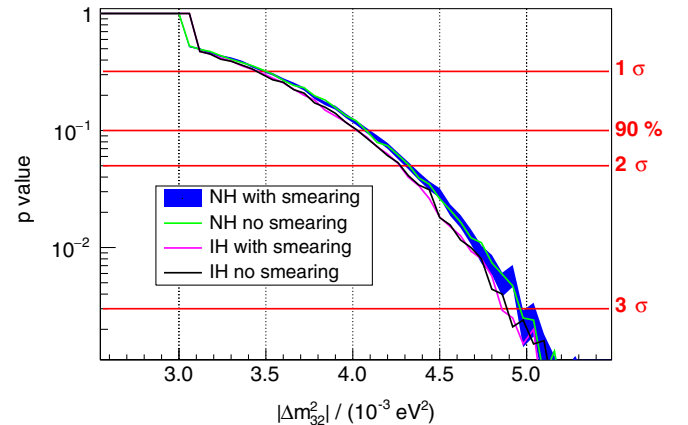


FIG. 2. p -values as a function of $|\Delta m_{32}^2|$, with all other oscillation parameters fixed to central values (Table 14.1 in [24]). Vertical width of the “NH with smearing” curve represents the 90% C.L. interval on p -value due to the finite numbers of pseudoexperiments; other curves have similar uncertainty which is not shown for clarity. p -values for $|\Delta m_{32}^2| < 2.5 \times 10^{-3}$ eV² are equal to 1 in all cases.

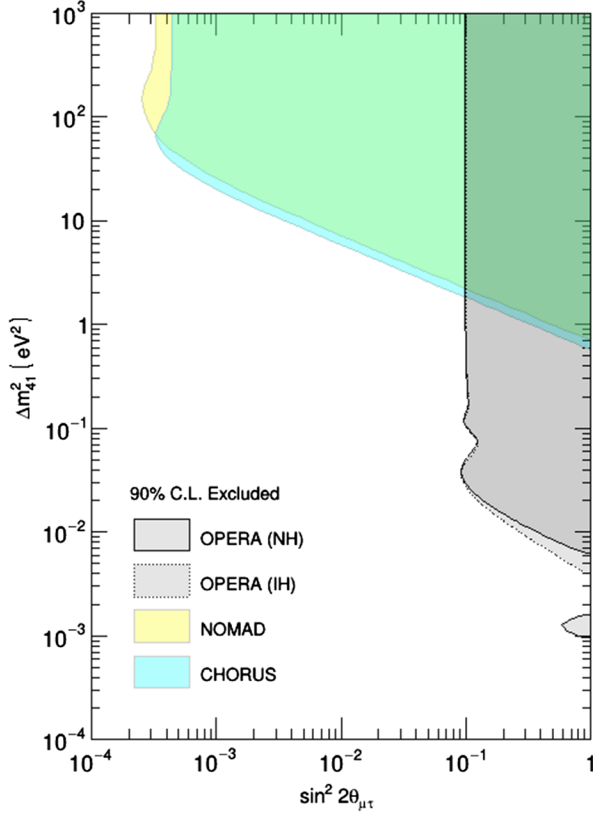


FIG. 3. OPERA 90% CL exclusion region in the Δm_{41}^2 and $\sin^2 2\theta_{\mu\tau}$ parameter space for the normal (NH, solid line) and inverted (IH, dashed line) hierarchy of the three standard neutrino masses. The exclusion regions by NOMAD [35] and CHORUS [36] are also shown.

B. Sterile 3 + 1 model

The excess of electron neutrino and antineutrino events reported by the LSND [18] and MiniBooNE [19] experiments may be interpreted as due to the presence of light $\mathcal{O}(1 \text{ eV})$ sterile neutrinos. OPERA can test this hypothesis searching for deviation from the prediction of the three-flavor neutrino model. The oscillation probability in this model depends on a four by four unitary mixing matrix U and three squared mass differences (Δm_{21}^2 , Δm_{31}^2 and Δm_{41}^2) [32].

Here, for the first time, tau and electron neutrino appearance channels are jointly used to test the sterile neutrino hypothesis in the framework of the 3 + 1 model. Since the NC-like over CC-like event ratio is poorly sensitive to the effects induced by the presence of a sterile neutrino state, the muon neutrino disappearance channel is not exploited in this analysis.

Defining $\sin^2 2\theta_{\mu\tau} = 4|U_{\tau 4}|^2|U_{\mu 4}|^2$, $\sin^2 2\theta_{\mu e} = 4|U_{e 4}|^2 \times |U_{\mu 4}|^2$ and Δm_{41}^2 as the parameters of interest, the profile likelihood ratio is used to remove the dependence of the likelihood [Eq. (1)] on the other parameters treated as nuisance. Exclusion regions of Δm_{41}^2 versus $\sin^2 2\theta_{\mu\tau}$ and $\sin^2 2\theta_{\mu e}$ are shown in Figs. 3 and 4, respectively. The result is restricted to positive Δm_{41}^2 values since negative values are

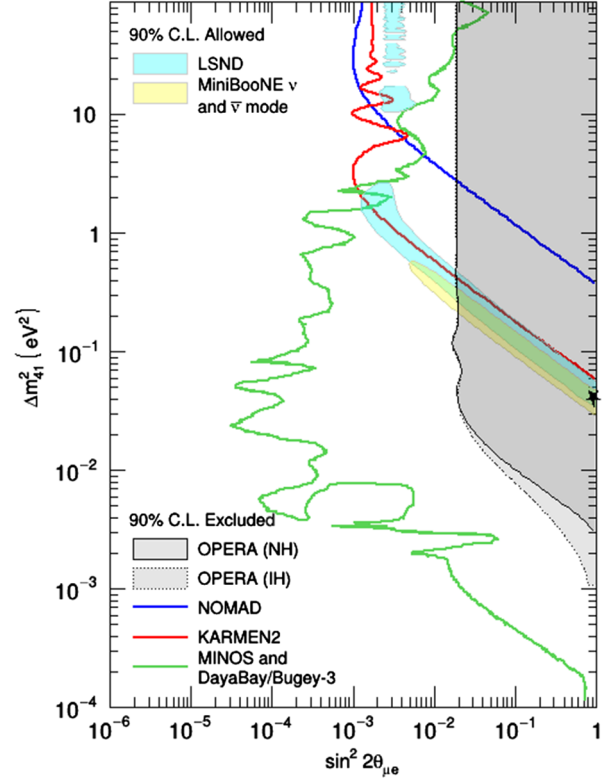


FIG. 4. The 90% C.L. exclusion region in the Δm_{41}^2 and $\sin^2 2\theta_{\mu e}$ plane is shown for the normal (NH, solid line) and inverted (IH, dashed line) hierarchy of the three standard neutrino masses. The plot also reports the 90% C.L. allowed region obtained by LSND [18] (cyan) and MiniBooNE combining ν and $\bar{\nu}$ mode [19] (yellow). The blue and red lines represent the 90% C.L. exclusion regions obtained in appearance mode by NOMAD [37] and KARMEN2 [38], respectively. The 90% C.L. exclusion region obtained in disappearance mode by the MINOS and DayaBay/Bugey-3 joint analysis [39] is shown as green line. The black star (*) corresponds to the MiniBooNE best-fit values for the combined analysis of ν and $\bar{\nu}$ data.

disfavored by results on the sum of neutrino masses from cosmological surveys [33]. The MINOS + Collaboration has recently reported an analysis setting limits on the existence of a sterile neutrino state [34].

For $\Delta m_{41}^2 > 0.1 \text{ eV}^2$, the upper limits on $\sin^2 2\theta_{\mu\tau}$ and $\sin^2 2\theta_{\mu e}$ are set to 0.10 and 0.019 both for the case of NH and IH. The limits obtained on the sterile oscillation parameters improve those reported in [16,17]. The values of the oscillation parameters ($\Delta m_{41}^2 = 0.041 \text{ eV}^2$, $\sin^2 2\theta_{\mu e} = 0.92$) corresponding to the MiniBooNE combined neutrino and antineutrino best-fit [19] are excluded with a p -value of 8.9×10^{-4} , corresponding to a significance of 3.3σ .

V. CONCLUSIONS

Searches for ν_τ and ν_e appearance and for ν_μ disappearance were performed using the full OPERA data sample.

The data are compatible with the three-flavor neutrino model and constraints on θ_{23} and θ_{13} were derived jointly for the first time exploiting tau and electron neutrino appearance channels. A best fit value of $\theta_{23} = 0.78_{-0.31}^{+0.32}$ rad at 1σ C.L. is obtained, while θ_{13} is constrained to $[0, 0.20]$ rad at 1σ C.L.

Additionally, a dedicated sample of OPERA electronic detector data is used to perform a search for the ν_μ disappearance signal in the CNGS beam. Assuming all other mixing parameters equal to the global fit central values (Table 14.1 in [24]), an upper limit $|\Delta m_{32}^2| < 4.1 \times 10^{-3} \text{ eV}^2$ at 90% C.L. is obtained.

Finally, ν_τ and ν_e appearance channels were combined for the first time to constrain parameters of the $3 + 1$ sterile mixing model. For $\Delta m_{41}^2 > 0.1 \text{ eV}^2$, upper limits on $\sin^2 2\theta_{\mu\tau}$ and $\sin^2 2\theta_{\mu e}$ are set to 0.10 and 0.019 for NH and IH. The MiniBooNE best-fit [19] values ($\Delta m_{41}^2 = 0.041 \text{ eV}^2$, $\sin^2 2\theta_{\mu e} = 0.92$) are excluded with 3.3σ significance.

ACKNOWLEDGMENTS

We warmly thank CERN for the successful operation of the CNGS facility and INFN for the continuous support

given by hosting the experiment in its LNGS laboratory. Funding is gratefully acknowledged from national agencies and Institutions supporting us, namely: Fonds de la Recherche Scientifique-FNRS and Institut Interuniversitaire des Sciences Nucleaires for Belgium; MZO for Croatia; CNRS and IN2P3 for France; BMBF for Germany; INFN for Italy; JSPS, MEXT, the QFPU-Global COE program of Nagoya University, and Promotion and Mutual Aid Corporation for Private Schools of Japan for Japan; SNF, the University of Bern and ETH Zurich for Switzerland; the Programs of the Presidium of the Russian Academy of Sciences (Neutrino Physics and Experimental and Theoretical Researches of Fundamental Interactions), and the Ministry of Education and Science of the Russian Federation for Russia, the Basic Science Research Program through the National Research Foundation of Korea (NRF) funded by the Ministry of Science and ICT (Grant No. NRF-2018R1A2B2007757) for Korea; and TUBITAK, the Scientific and Technological Research Council of Turkey for Turkey (Grant No. 108T324). We warmly acknowledge the important contributions given by our deceased colleagues G. Giacomelli, A. Ljubičić, G. Romano and P. Tolun.

-
- [1] R. Acquafredda *et al.* (OPERA Collaboration), *J. Instrum.* **4**, P04018 (2009).
- [2] G. Acquistapace *et al.*, CERN Reports No. CERN-98-02 and No. INFN/AE-98/05, <http://proj-cngs.web.cern.ch/proj-cngs/>.
- [3] R. Baldy *et al.*, CERN Reports No. CERN-SL-99-034-DI and No. INFN-AE-99-05, 1999; Addendum to CERN Reports No. CERN-98-02 and No. INFN/AE-98/05.
- [4] Y. Fukuda *et al.* (Super-Kamiokande Collaboration), *Phys. Rev. Lett.* **81**, 1562 (1998).
- [5] M. Ambrosio *et al.* (MACRO Collaboration), *Phys. Lett. B* **434**, 451 (1998).
- [6] N. Agafonova *et al.* (OPERA Collaboration), *New J. Phys.* **13**, 053051 (2011).
- [7] Yu. A. Gornushkin, S. G. Dmitrievsky, and A. V. Chukanov, *Phys. Part. Nucl. Lett.* **12**, 89 (2015).
- [8] M. Ambrosio *et al.*, *IEEE Trans. Nucl. Sci.* **51**, 975 (2004).
- [9] N. Agafonova *et al.* (OPERA Collaboration), *Phys. Rev. Lett.* **115**, 121802 (2015).
- [10] N. Agafonova *et al.* (OPERA Collaboration), *Phys. Lett. B* **691**, 138 (2010).
- [11] N. Agafonova *et al.* (OPERA Collaboration), *J. High Energy Phys.* **11** (2013) 036.
- [12] N. Agafonova *et al.* (OPERA Collaboration), *Phys. Rev. D* **89**, 051102 (2014).
- [13] N. Agafonova *et al.* (OPERA Collaboration), *Prog. Theor. Exp. Phys.* **2014**, 101C01 (2014).
- [14] N. Agafonova *et al.* (OPERA Collaboration), *Phys. Rev. Lett.* **120**, 211801 (2018); **121**, 139901(E) (2018).
- [15] N. Agafonova *et al.* (OPERA Collaboration), *J. High Energy Phys.* **07** (2013) 004; **07** (2013) 85.
- [16] N. Agafonova *et al.* (OPERA Collaboration), *J. High Energy Phys.* **06** (2018) 151.
- [17] N. Agafonova *et al.* (OPERA Collaboration), *J. High Energy Phys.* **06** (2015) 069.
- [18] A. Aguilar-Arevalo *et al.* (LSND Collaboration), *Phys. Rev. D* **64**, 112007 (2001).
- [19] A. A. Aguilar-Arevalo *et al.* (MiniBooNE Collaboration), *Phys. Rev. Lett.* **121**, 221801 (2018).
- [20] N. Agafonova *et al.* (OPERA Collaboration), *Eur. Phys. J. C* **74**, 2986 (2014).
- [21] C. Andreopoulos *et al.*, *Nucl. Instrum. Methods Phys. Res., Sect. A* **614**, 87 (2010).
- [22] C. Andreopoulos, C. Barry, S. Dytman, H. Gallagher, T. Golan, R. Hatcher, G. Perdue, and J. Yarba, [arXiv:1510.05494](https://arxiv.org/abs/1510.05494).
- [23] A. Bertolin and N. T. Tran (OPERA Collaboration), OpCarac: An algorithm for the classification of the neutrino interactions recorded by OPERA (2009), OPERA public note 100.
- [24] M. Tanabashi *et al.* (Particle Data Group), *Phys. Rev. D* **98**, 030001 (2018).
- [25] P. Huber, M. Lindner, and W. Winter, *Comput. Phys. Commun.* **167**, 195 (2005).
- [26] P. Huber, J. Kopp, M. Lindner, M. Rolinec, and W. Winter, *Comput. Phys. Commun.* **177**, 432 (2007).
- [27] A. Ferrari, A. M. Guglielmi, M. Lorenzo-Sentis, S. Roesler, P. R. Sala, and L. Sarchiapone, CERN Technical Report No. CERN-AB-Note-2006-038, 2007.

- [28] A. M. Dziewonski and D. L. Anderson, *Phys. Earth Planet. Interiors* **25**, 297 (1981).
- [29] F. D. Stacey, *Physics of the Earth*, 4th ed. (Cambridge University Press, Cambridge, England, 2008), <https://doi.org/10.1017/S0016756809006104>.
- [30] G. Cowan, K. Cranmer, E. Gross, and O. Vitells, *Eur. Phys. J. C* **71**, 1554 (2011); **73**, 2501(E) (2013).
- [31] B. Kliček, Ph.D. thesis, University of Zagreb, 2018.
- [32] M. Dentler, A. Hernandez-Cabezudo, J. Kopp, P. A. N. Machado, M. Maltoni, I. Martinez-Soler, and T. Schwetz, *J. High Energy Phys.* **08** (2018) 010.
- [33] P. A. R. Ade *et al.* (Planck Collaboration), *Astron. Astrophys.* **594**, A13 (2016).
- [34] P. Adamson *et al.* (MINOS+Collaboration), *Phys. Rev. Lett.* **122**, 091803 (2019).
- [35] P. Astier *et al.* (NOMAD Collaboration), *Nucl. Phys.* **B611**, 3 (2001).
- [36] E. Eskut *et al.* (CHORUS Collaboration), *Nucl. Phys.* **B793**, 326 (2008).
- [37] P. Astier *et al.* (NOMAD Collaboration), *Phys. Lett. B* **570**, 19 (2003).
- [38] B. Armbruster *et al.* (KARMEN Collaboration), *Phys. Rev. D* **65**, 112001 (2002).
- [39] P. Adamson *et al.* (MINOS and Daya Bay Collaborations), *Phys. Rev. Lett.* **117**, 151801 (2016); **117**, 209901(A) (2016).